15 Aug 2008, 3:30 pm - 4:15 pm

Bearing Capacity Evaluation of Long, Large-Diameter, Open-Ended Piles

Yoshiaki Kikuchi

Port & Airport Research Institute, Yokosuka, Japan


6th International Conference on
Case Histories in Geotechnical Engineering, Arlington, VA, August 11-16, 2008

BEARING CAPACITY EVALUATION OF LONG, LARGE-DIAMETER, OPEN-ENDED PILES

Yoshiaki Kikuchi
Port & Airport Research Institute
Yokosuka, JAPAN

ABSTRACT

Recent changes in port construction in Japan include the use of deeply embedded large-diameter steel pipe piles. However, little change has been made to the procedure for estimating the bearing capacity of piles. An international comparison of bearing capacity estimation techniques and examination of the bearing capacity mechanism of open-ended piles were conducted. In this study, the plugging phenomenon was thoroughly investigated by means of field loading tests, large- and small-scale laboratory experiments with X-ray CT scanner, and numerical analysis.

INTRODUCTION

For the past 50 years, the pile foundations of port facilities in Japan have been constructed by means of driving steel pipe piles. Although pile diameter and length have been modified over the years, the design method has hardly changed. Furthermore, the evaluation of bearing capacity at the pile toe has always been a problem. The recent use of large-diameter open-ended piles has created considerable uncertainty about the toe bearing capacity. This problem has been taken into account in the design as a plugging ratio. However, the argument in the estimation method for the plugging ratio is not sufficient. The opportunity for re-examination of the bearing capacity of a pile is growing from recent arguments for introduction of performance-based design and international compatibility of design methods. Accordingly, this paper introduces the changes adopted for pile foundations used in Japan's port facilities and presents the conditions of the bearing-capacity estimation method for piles, worldwide trends in bearing-capacity estimation methods, and the latest studies on the bearing capacity at the toe of open-ended piles.

PREVIOUS STUDIES

For precise estimation of the point bearing capacity of open-ended piles, it is important to evaluate the plugging effect at the bottom tip of the pile. Therefore, many analytical and experimental studies have already been conducted on the plugging mechanism of open-ended piles. As a result of those studies, various suggested algorithms have been adopted in several design codes in Japan, such as the Specifications for Highway Bridges (Japan Road Association 2002) and Recommendations for the Design of Building Foundations (Architectural Institute of Japan 2001). In Recommendations for the Design of Building Foundations, the point bearing capacity of the open-ended pile is evaluated as being equal to ηR_{PC}, in which R_{PC} indicates the point bearing capacity of the closed-end pile, and η is a coefficient of the plugging effect. If L_B/d_I, which is the ratio of embedded depth in stiff layer (L_B) to the pile diameter (d_I), is less than 5, η is equal to 0.16 (L_B/d_I), and in cases where L_B/d_I is greater than 5, then η is equal to 0.8.

Thus, it has been assumed that the conditions for plugging effect depend on the ratio of embedded depth to pile diameter. In cases where the embedded depth is less than the regulation, the point bearing capacity of the open-ended pile is reduced at a fixed rate unrelated to the ground characteristics at the construction site. This could be one of the causes of underestimation of the point bearing capacity of open-ended piles.

PRESENT STATE OF PILE FOUNDATIONS IN PORT AREAS OF JAPAN

The design situation from 1961 to 1965 was investigated in 1967 (Kitajima et al.). At that time, the material used for the piles in 54 open piers consisted of steel pipe (80% of the piles) and H steel (11% of the piles). That is, about 90% of the piles were steel piles. When 100 examples of pile foundation designs from 1989 to 2001 were investigated in 2003, it was found that 97% were steel pipe piles. The only piles not made of steel were those used for the bridge pier of a port road. This shows that most foundation piles of port facilities are steel piles.

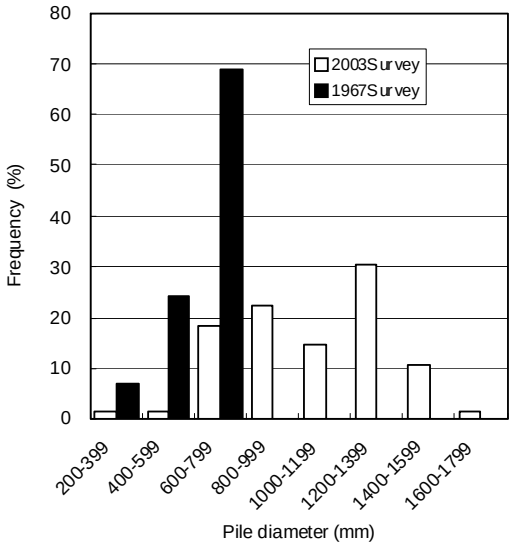

Fig. 1. Change in pile diameter.

Change in distribution of the pile diameter of steel pipe piles by these two investigations is shown in Fig. 1. These results show that piles with a diameter of about 1300 mm have been in use in recent years, whereas piles with a diameter of 800 mm or less were used in the 1960s.

Distribution of the embedded length of piles is shown in Fig. 2. The embedded length of some piles exceeds 60 m in recent years, whereas it was about 30 m in the 1960s.

The necessity for large bearing capacity piles to support increased loads from enlargement of super structures and improvement in construction technology and equipment have influenced the above changes. The change in pile diameter and embedded length requires a change in the static bearing capacity estimation equation used for the design.

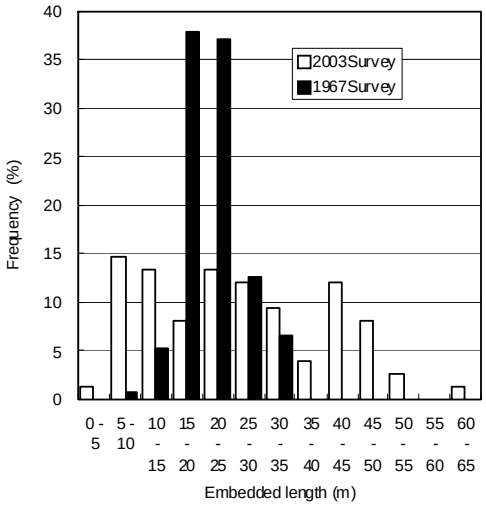

Fig. 2. Change in embedded length.

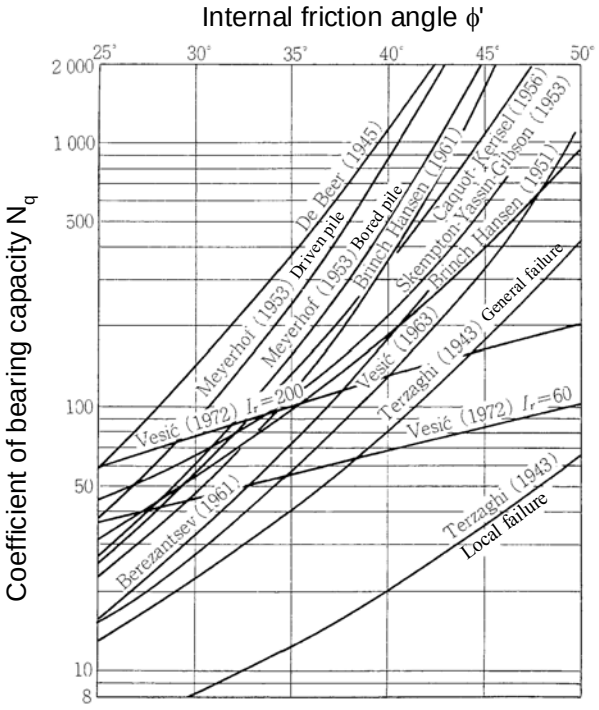

Fig. 3. Relationship between Nq and ϕ proposed by researchers.

INTERNATIONAL COMPARISON OF PRESUMED STATIC BEARING CAPACITY OF PILES

The bearing capacity of a single pile is commonly divided into toe bearing capacity and shaft resistance force (Fleming et al., 1992).

The calculation formulae for static bearing capacity of piles used in the port construction standards of Japan (JPTS), and Eurocode7 (EC7) and the standard for the U.S. Army Corps of Engineers (USCOE) as a typical example of the calculation

Table 1. Comparison of static bearing capacity calculation methods in each design code

		JPTS	Eurocode7 (EC7)	USCOE
Sandy ground	Base resistance q_p(kN/m^2)	$300N$	$N_q\sigma_{v0}'$	$N_q\sigma_{v0}'$
	Shaft resistance q_s(kN/m^2)	$2N$	$K_s\ \sigma_{v0}'\tan\delta$	$K_s\ \sigma_{v0}'\tan\delta$
Clayey ground	Base resistance q_p(kN/m^2)	$8c_u$	$9c_u+\ \sigma_{v0}'$	$9c_u$
	Shaft resistance q_s(kN/m^2)	c_u	αc_u	αc_u

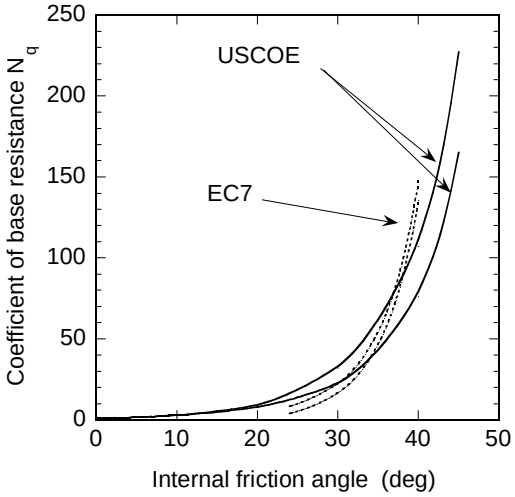

Fig. 4. N_q used in EC7 and USCOE.

formula, are compared in Table 1 (OCDI, 2002; Orr and Farrell, 1999; ASCE, 1993). As shown in the table, in every standard, the bearing capacity calculation condition of a pile is divided into a sandy layer and a clayey layer. Moreover, bearing capacity is separated into shaft resistance and toe resistance.

In JPTS, the SPT-N value is used for estimating the bearing capacity of piles in sandy ground. For piles in clayey ground, the shear strength from an unconfined compression test is used. A similar estimation method is used for the bearing capacity of piles both in EC7 and USCOE. That is, the toe bearing capacity of a pile in sandy ground is estimated by the product of the coefficient of bearing capacity and the overburden pressure. The shaft resistance is assumed to be proportional to the normal stress at the pile surface. The bearing capacity of the pile in clayey ground is estimated based on the undrained shear strength in each code.

This comparison shows that bearing capacity estimation for a pile in clayey ground is similar in the three codes. However, the bearing capacity estimation methods for a pile in sandy ground differ greatly. The method in JPTS is originally what Meyerhof (1956) proposed from the relationship between unit toe resistance and SPT-N value (q_p = 400 N). However, the constant of the equation is modified in many instances in Japan (Yamagata, 1975) and shaft resistance is proposed based on many measurement examples (Yamagata, 1975). Thus, the bearing capacity estimation technique in JPTS mainly relies on experiential results.

The coefficient of bearing capacity N_q for estimating toe bearing capacity of a pile in sandy ground used in EC7 and USCOE is calculated by supposing the failure mechanism of the ground around the pile toe. The bearing capacity coefficient N_q is determined from the internal friction angle ϕ. Although this method is rational, the coefficient of bearing capacity varies with the assumption of a failure mechanism

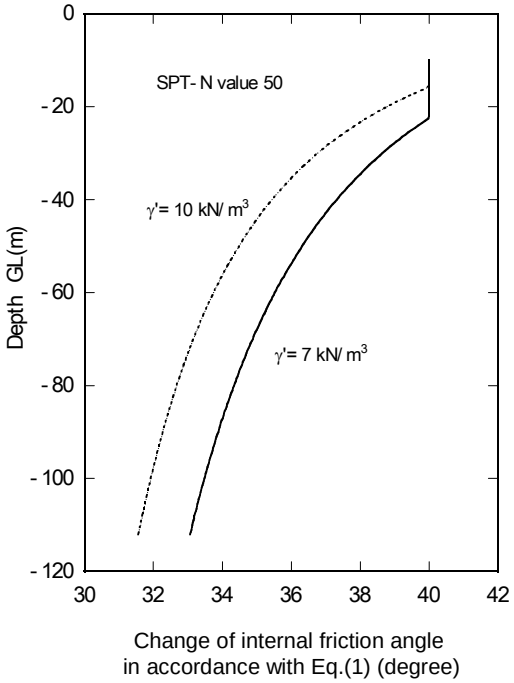

Fig. 5. Internal friction angle calculated with Eq. (1).

that is more than 10 times greater. For this reason, the relationship between Nq and ϕ proposed by many researchers varies greatly (Fig. 3) (Japanese Geotechnical Society, 1999). Moreover, there is a difference in the assumption of effective overburden pressure. In EC7, it is assumed that all overburden pressures are effective. On the other hand, in USCOE, it is proposed that the effective overburden pressure in bearing capacity calculation of a deeply embedded pile should be reduced from the total overburden pressure according to the proposal by Meyerhof (ASCE, 1993).

Shaft resistance force is premised on the frictional resistance along a shaft, and such an assumption is rational. However, it is difficult to precisely determine the earth pressure coefficient at the pile shaft.

Coefficients of bearing capacity Nq shown in Fig. 4 are used in EC7 and USCOE. They give moderate numbers comparing the variance of N_q shown in Fig. 3. Internal friction angle should be defined when calculating N_q. Here, the following equation is used for estimating the internal friction angle from the SPT-N value and is introduced in the present JPTS. This equation is constructed from two proposals by Meyerhof (1957, 1959) about the relationship between SPT-N value and relative density and between relative density and internal friction angle. If this equation is used, ϕ will become smaller if the depth increases under the condition of the SPT-N value independent from the depth, as shown in Fig. 5.

$$\phi = 25 + 3.2\sqrt{\frac{100N}{p'_{v0} + 70}} \qquad (1)$$

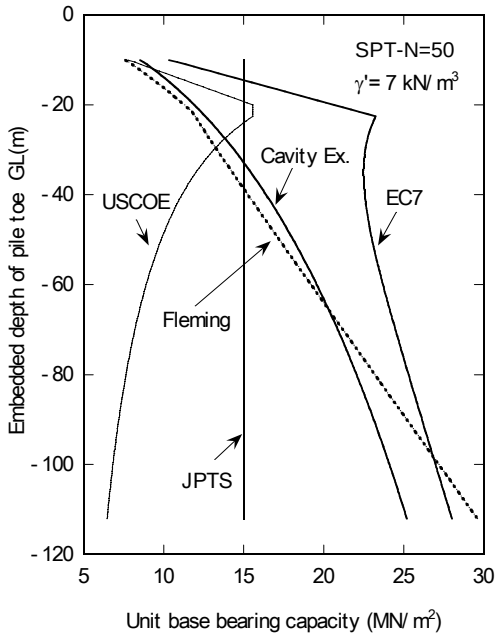

Fig. 6. Comparison of toe bearing capacity in JPTS, EC7, and USCOE.

where N: SPT-N value and p'_{v0} : effective overburden pressure at sounding.

Although the toe bearing capacity per unit area is determined by only the SPT-N value using the method in JPTS, it is determined from the SPT-N value and effective unit volume weight in EC7 and USCOE. Furthermore, in USCOE, the maximum effective overburden pressure is considered to be affected by the pile diameter and ground conditions.

Other methods for estimating the bearing capacity of piles are presented. In one method, proposed by Fleming (1992), the same bearing capacity coefficient N_q as EC7 is used. However, how to obtain the internal friction angle differs from the above-mentioned method. The internal friction angle used for determining N_q is shown by the following formula:

$$\phi' = \phi_{cv}' + 3I_R \quad \text{(degrees)} \tag{2}$$

where ϕ_{cv}' : critical state friction angle, I_R: corrected relative density calculated from $I_R = I_D(5.4 - \ln(p'/p_a)) - 1$ (if p' < 150 kPa) or $I_R = 5I_D - 1$ (if p' > 150 kPa), I_D: uncorrected relative density, p': mean stress level calculated from $p' = \sqrt{N_q} \cdot \sigma_v'$, p_a: atmospheric pressure (100 kPa), σ_v' : effective vertical stress.

Another method is the cavity extension theory. This theory used for estimating the bearing capacity of a pile was originally proposed by Vesic (1972). Yasufuku et al. (2001) revised it as follows:

$$q_p = \frac{3(1+\sin\phi_{cv}')}{(1-\sin\phi_{cv}')(3-\sin\phi_{cv}')}\left[I_{rr}\right]^{(4\sin\phi_{cv}'/(3(1+\sin\phi_{cv}')))}\left(\frac{3-2\sin\phi_{cv}'}{3}\right)\sigma_{v0}' \tag{3}$$

$$I_{rr} = \frac{I_r}{1 + I_r\Delta_{av}} \tag{4}$$

$$I_r = \frac{3G}{(3-\sin\phi_{cv}')\sigma_{v0}'\tan\phi_{cv}'} \tag{5}$$

where q_p: unit bearing capacity of pile toe (kN/m^2)
I_{rr}: reduced rigidity index
I_r: rigidity index
ϕ_{cv}' : critical state friction angle (degrees), which can be $\phi_{cv}' = 30 + \Delta\phi_1 + \Delta\phi_2$. Values of $\Delta\phi_1$ and $\Delta\phi_2$ can be referred from Table 2.
Δa_v: average volumetric strain for plastic zone around a cavity. It is a function of I_r: $\Delta_{av} = 50(I_r)^{-1.8}$.
G: shear stiffness, which can be calculated from G = 7000 $N^{0.72}$(kN/m^2). N is the SPT-N value around a pile toe.

Figure 6 shows the difference in estimated toe bearing capacity using these five methods. Here, the SPT-N value is assumed to be 50 independent of the depth and it means that the ground is assumed to be a uniform, dense sandy layer. Effective unit weight of the ground is assumed to be 7 kN/m^3. In this case, according to the USCOE code, if the embedded depth is at least 20 times greater than the pile diameter, the effective overburden pressure in bearing capacity estimation will become constant at 20Dγ'.

Table 2. $\Delta\phi_1$ and $\Delta\phi_2$ for sandy soil and gravel

Angularity	$\Delta\phi_1$(°)	Grading of soil	$\Delta\phi_2$(°)
Round	0	Uniform (U_c < 2)	0
Sub-angular	2	Moderate grading (2 < U_c < 6)	2
Angular	4	Well graded (6 < U_c)	4

The estimated toe bearing capacity using JPTS is independent of the embedded depth, as shown in Fig. 6. This has an odd effect in that the bearing capacity does not change in the depth direction. Methods proposed by Fleming and Yasufuku almost coincide at depths shallower than 50 m, but they are discrepant at deeper parts. EC7 shows the highest bearing capacity at almost all depths. However, estimated bearing capacities by the five methods become almost the same when the embedded depth of the piles is 15–40 m and they show a big difference when the embedded depth is deeper.

The measured value was compared with the estimated value. From now on, estimated values by JPTS and EC7 and the cavity expansion method are used for comparison of the bearing capacity of piles. Figure 7 a) shows a comparison between the measured toe bearing capacity per unit area and the estimated value in the case of a pile diameter of 1000 mm or less. The measured data used for this comparison is from the Japanese Association for Steel Pipe Piles (JASPP 2000) and the

latest data. This result shows that the measured values are smaller than the estimated values. The estimated values by JPTS and the cavity expansion method become closer to the measured values compared to those by EC7. However, when the embedded depth of the pile becomes deep, the values using JPTS were underestimated compared to the measured values.

Figure 7 b) shows the same type of comparison for the case of a pile diameter of 1000 mm or more. It turns out that the measured values are considerably smaller than the estimated values on the whole. This is because forming of the plug of a pile toe portion becomes inadequate and the bearing capacity is smaller than the calculated bearing capacity based on a closed-end pile, when the pile diameter becomes large.

Since the toe resistance at the plug portion of an open-ended

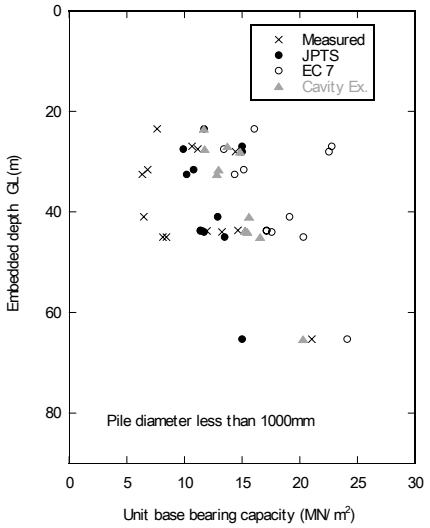

a) Pile diameter 1000 mm or less

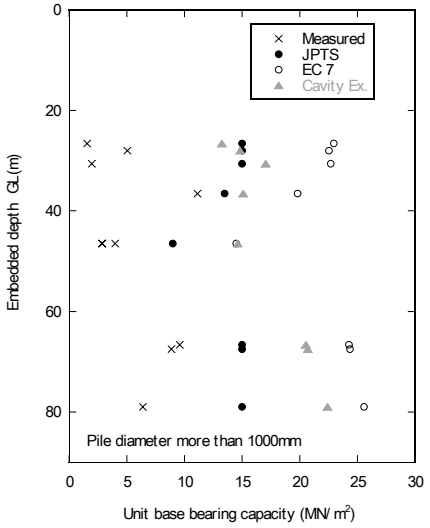

b) Pile diameter 1000 mm or more

Fig. 7. Comparison between measured and estimated bearing capacity.

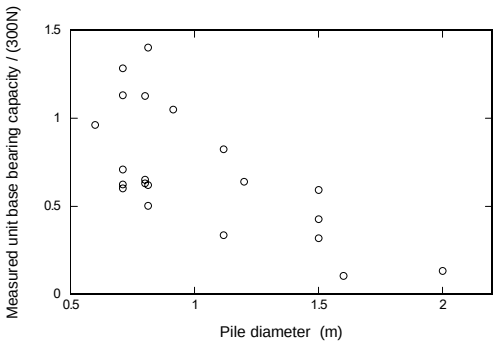

Fig. 8. Relationship between pile diameter and the ratio of measured and estimated bearing capacity.

pile may decrease if the pile diameter is increased, it is possible that the resistance at the real portion of the pile will differ from that of the plug portion even if the pile diameter is 1000 mm or less. When considered in this way, there is no reason to believe that even the EC7 results are overestimated or that the JPTS results are preferable for estimating measured data.

As described in PRESENT STATE OF PILE FOUNDATIONS IN PORT AREAS OF JAPAN, most piles presently used in port facilities are deeply embedded large-diameter steel pipe piles. When estimating the bearing capacity of this type of pile, the toe bearing capacity poses a big problem, referred to as the problem of plugging ratio.

Figure 8 provides a reference for considering the plugging of a large-diameter steel pipe pile. The figure shows the relationship between the pile diameter and the ratio of measured toe resistance and the estimation results of JPTS. Since the embedded depth is not considered in the figure, the data shows some variation, but it is clear that there is a tendency for the toe bearing capacity of the pile per unit area to be small when the pile diameter is large. This means that the resistance per unit area of the portion of a plug becomes small when the pile diameter becomes large.

EXAMINATION OF BEARING CAPACITY MECHANISM OF OPEN-ENDED PILES

The Tokyo Port Seaside Road was designed so that the Tokyo Coastal Highway Bridge would cross over Channel No. 3 of the port. The subject of this study is a steel-pipe-sheet pile foundation that features large-diameter steel pipe piles serving as the pier foundation between the principal meridians of the Tokyo Coastal Highway Bridge. As its bearing capacity has not been fully proved, load tests (including a static axial compressive load test, rapid load test, and dynamic load test) were conducted, as shown in Fig. 9, to obtain information about the bearing mechanism of the foundation piles at the site of the planned bridge construction, and the test results were used for designing the bridge. The characteristics of vertical bearing

Fig. 9. View of static axial compressive load test.

capacity obtained from in-situ tests on actual size large-diameter open-ended steel pipe piles are discussed here.

Overview of static axial compressive load test

Figure 10 shows the ground conditions where the tests were conducted and the embedded depth of test piles. It can be seen from the figure that the water depth at this site is AP-7 m. A soft, cohesive alluvium layer continues down to AP-40 m, followed by laminated ground (alternating sandy and cohesive layers) down to AP-65 m, and then a diluvial sandy gravel layer (Tokyo gravel layer) appears around AP-69 m. Following a few weak layers in the sandy gravel layer around AP-80 m, a solid sandy layer appears around AP-82 m.

The results of static axial compressive load tests are presented here. In the tests, steel pipe piles 1,500 mm in diameter were hammer-driven into a sandy gravel layer and a sandy layer, in

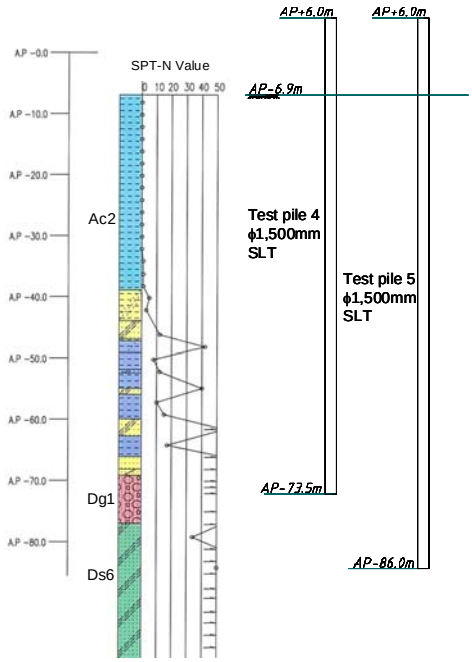

Fig. 10. Overview of soil boring log and embedment of test piles.

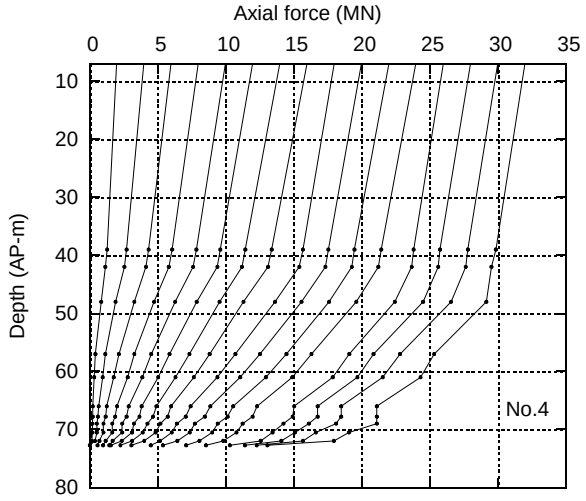

Fig. 11. Axial force distribution in Pile No. 4 load test.

order to obtain the characteristics of bearing capacity under two conditions (in sandy gravel layer and sandy layer).

In these load tests, the axial force acting on a pile was measured by attaching strain gauges to the pile; at the same time, the settlement of the pile (both at the toe and the head) was measured using settlement gauges. Multi-stage repeated loading was conducted in accordance with the static axial compressive load test method proposed by the Japanese Geotechnical Society (2002). Particular care was taken when a virgin load was applied; that is, the load was maintained for 30 min or longer to wait for settlement of the pile, before moving to the next loading stage.

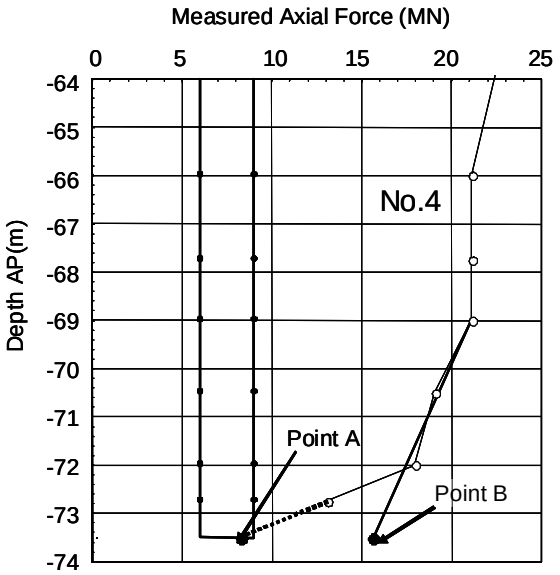

Fig. 12. Axial force distribution at the base of Pile No. 4.

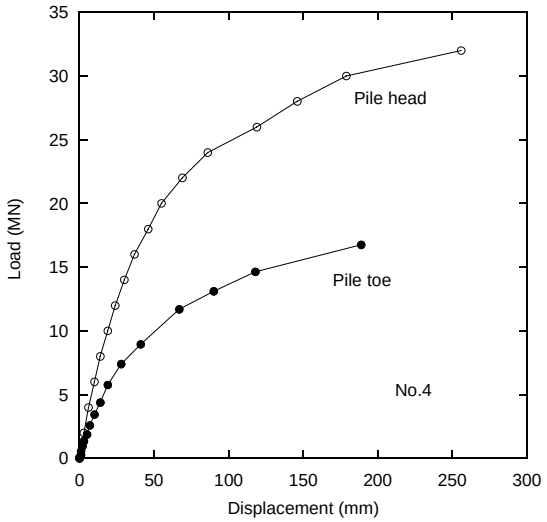

Fig. 13. Relationship between load and displacement on Pile No. 4.

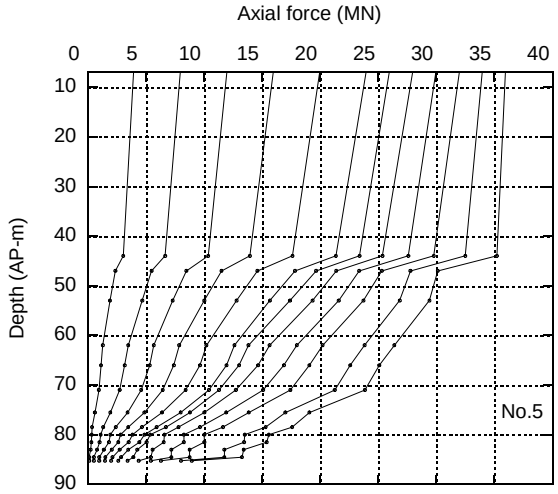

Fig. 14. Axial force distribution in Pile No. 5 load test.

Vertical bearing capacity

Figure 11 shows the axial force distribution when a virgin load was applied to Pile No. 4. What should be noted here is the axial force distribution around the lower end of the test pile. As the lower end was being embedded into the sandy gravel layer, the subgrade resistance increased, with a large change in the axial force in the depth direction. At the point where the pile head load exceeded 22,000 kN, the axial force distribution showed a large bend around the pile toe. This suggests that transferred axial pile force rapidly decreased toward the pile toe.

Figure 12 shows an enlarged view of the situation around the pile toe. Here, assuming the load at Point B in Fig. 12 to be the toe resistance, load settlement curves for both the head and lower end of the pile can be obtained as shown in Fig. 13.

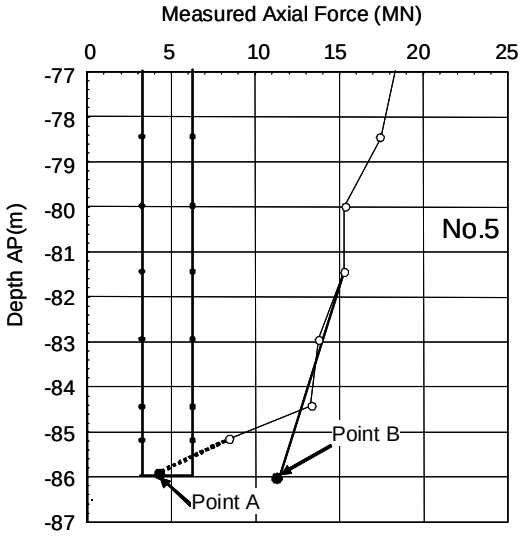

Fig. 15. Axial force distribution at the base of Pile No. 5.

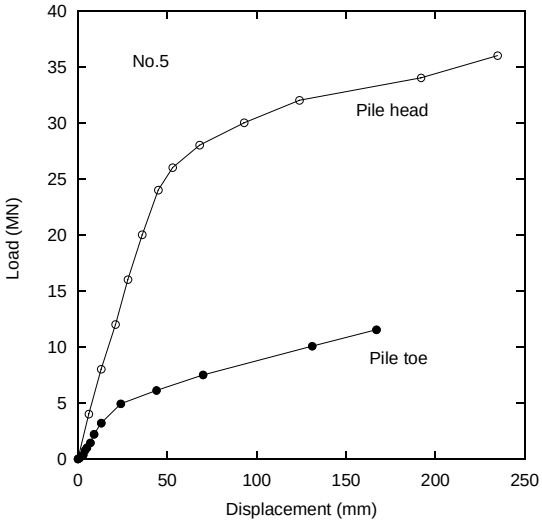

Fig. 16. Relationship between load and displacement on Pile No. 5.

Table 3. Critical resistance (MN).

	Pile No. 4	Pile No. 5
Primary critical resistance	20	26
Secondary critical resistance	32	36

The loading test results for Pile No. 5 are shown in Figs. 14 to 16. Although the embedded length differed from Pile No. 4, the pile was inserted into a stiff sandy layer. The features of the axial force distribution were similar to the results of the load test on Pile No. 4, such that the transferred axial pile force rapidly decreased toward the pile toe when the load applied to the pile head was close to the bearing capacity.

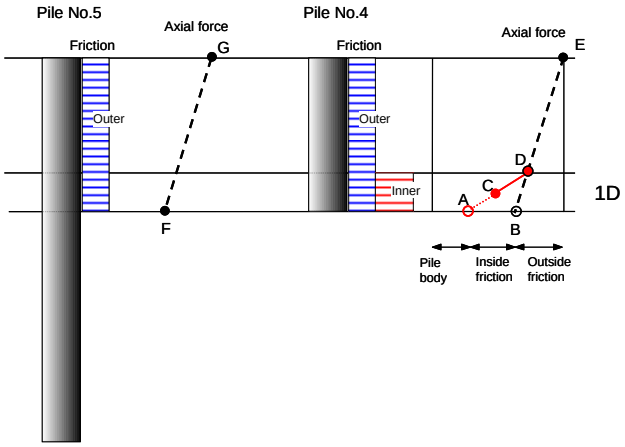

Fig. 17. Relationship between axial force distribution and friction.

Based on the relationship between vertical axial compressive load and pile displacement shown in Figs. 13 and 16, the primary and secondary critical resistance (when the toe displacement is 10% of the pile diameter) were obtained as shown in Table 3.

End bearing capacity of pile

The axial force distribution around a pile end under the secondary critical resistance is shown in Figs. 12 and 15. Axial force suddenly became smaller than at the upper part at the point where the strain gauge was set near the lower pile end. The point showing a sharp change in axial force was 1D (D: pile diameter) above the lower pile end.

Focusing on the phenomena at the pile toe of No.4 pile, ground solidity did not change around the lower pile end, Judging from the test results for Pile No. 5 that was more deeply embedded, it was unlikely that peripheral friction became large only at this point (see Fig. 17). Moreover, the results of a cone penetration test (CPT) showed that the penetration resistance of the inner soil at the pile base clearly became larger than the outer ground after the loading test as shown in Fig. 30. Thus, it can be concluded that a sharp change in axial force might have been caused by skin friction at the inner side of the pile. As shown in Fig. 17, the total bearing capacity at the pile toe could be obtained by extrapolating the measured values of axial force within the assumed bearing layer to the level of the lower pile end (Point B).

Assuming that the load at Point A obtained by extrapolating the measured value that curved at the pile end should be the resistance of the pile body, the difference between the load at Point B and the load at Point A could be regarded as the plug resistance due to inner friction. Figures 18 and 19 show the relationship between total base resistance, inner friction resistance, and resistance of the pile body. In both figures, at the

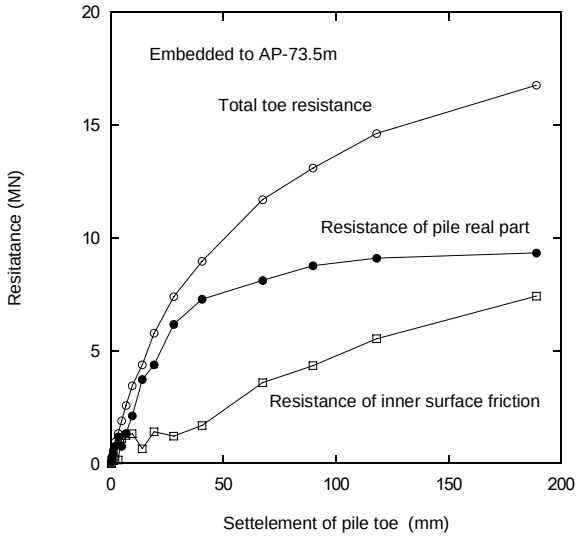

Fig. 18. Resistance at base of Pile No. 4.

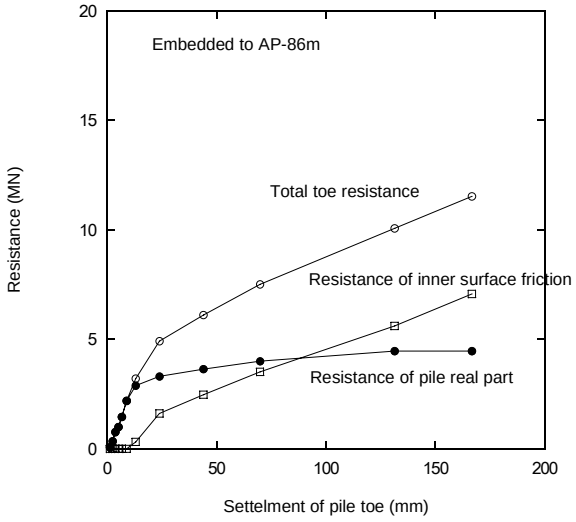

Fig. 19. Resistance at base of Pile No. 5.

secondary critical resistance, the total base resistance shows an increase. The resistance of the pile body reached nearly the maximum level when the settlement of the pile end was about 50 mm, about 3% of settlement, while inner friction resistance was still increasing.

Yamagata and Nagai (1973) and Nicola and Randolph (1997) proposed an equation to obtain the ultimate resistance of a unit sectional area, based on their assumption that the base resistance of the open-ended pile can be expressed as the sum of resistance at the sectional area of the lower end of a pile, A_t, and inner friction.

Yamagata and Nagai (1973) proposed the following equation to estimate this resistance from the SPT-N value: $q_t = 0.4NA_t$

(MN/m^2).

From the loading test results for a full-scale open-ended pile, Nicola and Randolph (1997) proposed a correlation between the resistance of the real portion of an open-ended pile, q_t, and CPT resistance, q_c:

$$q_t = \left(\frac{\lambda m (w_t / D)}{(w_t / D) + c} \right) q_c A_t \quad (6)$$

where m = 0.7, c = 0.015, w_t/D: normalized settlement of the pile toe.

λ: = 1.75 − (σ'_v/200) ($\sigma'_v \leq 200$ kPa)

= 0.75 ($\sigma'_v \geq 200$ kPa)

When converting the equation proposed by Nicola and Randolph under the test pile embedment condition and the secondary critical load condition, the resistance of the unit sectional area q_b can be obtained from the cone penetration resistance q_c as follows: $q_b = 0.46 q_c$ (kN/m^2). Thus, the ultimate resistance R_t of the sectional area of a pile can be obtained using the proposed equations, based on the SPT-N value measured at the pile base and the CPT results, as shown in Table 4.

The loads at Point A on Pile No. 4 and No. 5 in Figs 12 and 15 under the secondary critical load condition were 8.2 and 4.6 MN, respectively, as shown in Figs. 18 and 19. Both loads were close to the R_t values shown in Table 4.

It might appear less accurate to assume that the end bearing capacity of a pile at Point C, where was the nearest axial force measuring point from the pile toe, is the sum of the resistance of the sectional area of the pile end and the inner friction, and that the load at Point B is the resistance of the sectional area of the pile toe, as shown in Fig. 17. However, the results coincide relatively well with the existing proposals, so the above assumption can be considered to be fairly correct. Table 5 shows the results obtained from load tests. Inner friction resistance was estimated to be 7.5 MN on Pile No. 4 (accounting for 48% of the end bearing capacity of the pile) and 6.7 MN on Pile No. 5 (accounting for 59% of its bearing capacity). Inner friction resistance showed similar values whether the bearing layer was the sandy gravel layer or the sandy layer. Thus, it can be said that the difference in pile base resistance under the secondary critical load in a sandy gravel layer and a sandy layer largely depends on the difference in pile body resistance.

Table 4. Resistance at sectional area of pile end R_t (MN)

Proposed by	Yamagata and Nagai (1973)		Nicola and Randolph (1997)	
R_t proposed equation	$0.4NA_t$		$0.46q_cA_t$	
Pile No.	4	5	4	5
Ground strength measured at pile toe	Converted SPT-N value (125)	Converted SPT-N value 68	CPT: q_c value 97 MPa	CPT: q_c value 50 MPa
Resistance R_t	(8.6)	4.7	7.7	4.0
Load at Point B	8.2	4.6	8.2	4.6

As shown in Table 4, the pile body resistance depends on the penetration resistance (CPTq_c value or converted SPT-N value) of a relatively limited area around the pile base. However, the inner friction in a sandy gravel layer and a sandy layer can apparently be determined independently regardless of the penetration resistance.

The loading test results show that the toe resistance could be divided into inner friction and resistance of the pile body. It is also shown that the maximum resistance of the pile body can be reached with a relatively small settlement, whereas a large settlement is required for exhibiting inner resistance.

Table 5. Bearing capacity at pile toe based on results of static axial compression load test

	Pile No. 4	Pile No. 5
Pile diameter (mm)	ϕ1,500	ϕ1,500
Type of bearing layer	Gravel	Sand
Embedded depth into bearing layer	3D (4.5m)	3D (4.5m)
Axial force at the gauge position at the lower end of pile (MN)	13.0	9.0
Bearing capacity at pile base (MN)	15.7	11.3

PENETRATION EXPERIMENT OF OPEN-ENDED PILES IN MODEL GROUND

To examine the plugging effect, a series of penetration experiments was performed on open-ended piles in model ground. In this series, bearing capacity and change in ground strength around the pile were observed. To observe the change in ground strength, cone penetration tests were conducted inside and outside the pile.

Material and experimental procedure

The model ground consisted of Souma sand #4 having a density of soil particles equal to 2.644 g/cm^3, and maximum and minimum void ratios of 0.634 and 0.970, respectively. Figure 20 displays the grain size distribution. Dried Souma sand was packed into a container 6 m in length, 3 m in width and 3 m in depth, through a pipe 3 cm in diameter. The height of the sand was kept at 1 m during sample preparation. The relative density of the model ground was about 40%.

After completing the sample preparation, model piles were driven into the ground. The piles were 20 cm in diameter and about 2 m in length, and were made of acrylic resin. A model pile could be used as either a closed-end or open-ended pile by attaching or removing a bottom plate, as shown in Fig. 21.

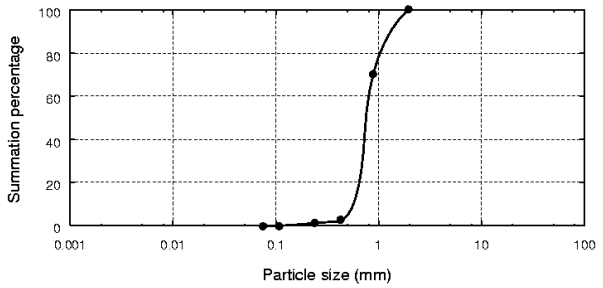

Fig. 20. Grain size distribution curve of Souma sand #4.

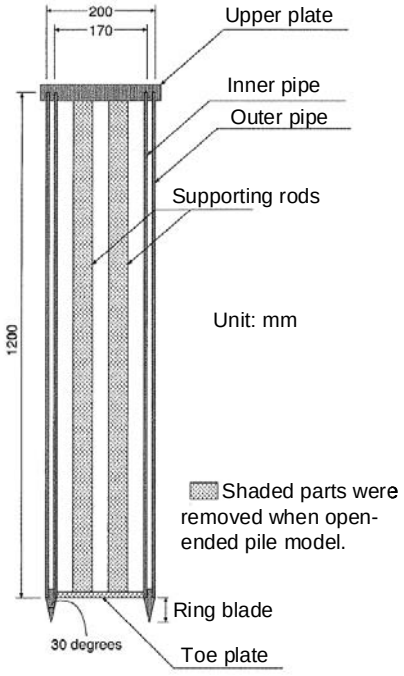

Fig. 21. Vertical cross section of model pile used in experiments.

The piles were driven into the model ground statically at a speed of 20 mm a minute. Penetration resistance at the pile head and height change of the surface of the ground inside open-ended piles were measured continuously during penetration.

After the installation of model piles, cone penetration tests were conducted around the piles. In addition, cone penetration tests have been performed at the center of the inside ground of the open-ended piles. The cones and rods originally designed for a portable cone penetrometer were applied in this series of model tests. The point angle of the cone is equal to 30° and the area of the base is equal to 3.24 cm^2. The diameter and length of rods are 16 mm and 500 mm, respectively. The cone was pushed into the ground at a speed of 7 mm/sec until the cone reached about 2.5 m in depth, and cone penetration resistance was measured continuously by a load cell.

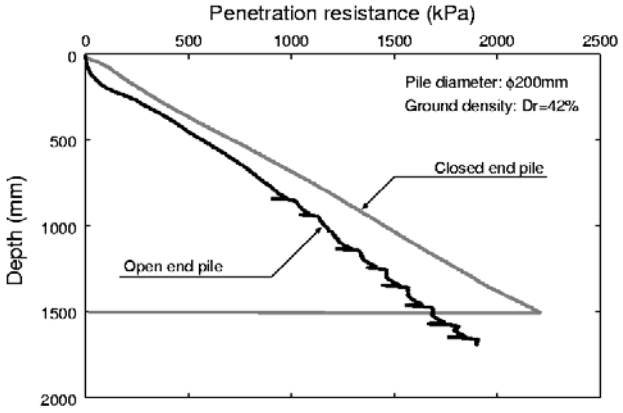

Fig. 22. Relationship between depth and penetration resistance.

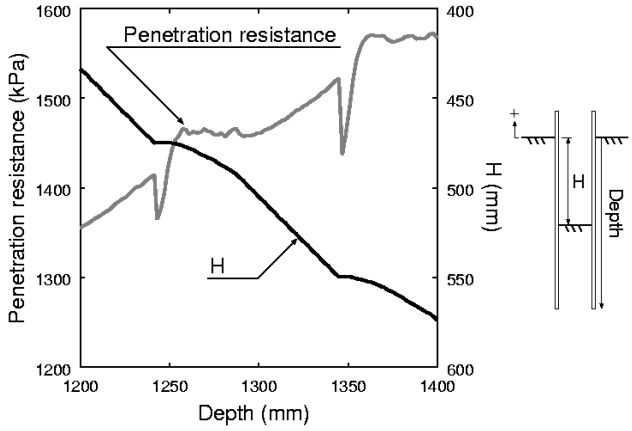

Fig. 23. Cyclic changing of penetration resistance of open-ended pile compared with height change of inside ground.

Behavior of model piles

Figure 22 shows the relationship between the depth and the penetration resistance of the model piles. In the case of the close-ended pile, the penetration resistance increased immediately after the onset of pile driving, while in the case of the open-ended pile, resistance increased gradually. After the penetration depth reached 800 mm, a remarkable change occurred in penetration resistance of the open-ended pile; that is, penetration resistance increased and decreased periodically.

An enlarged cycle of this periodical change in penetration resistance is displayed in Fig. 23, compared with the height change of the inside ground surface of the open-ended pile. The cyclic behavior included four phases: 1) A sudden reduction in penetration resistance took place at about 1250 mm in depth. At that moment, the height change of the inside ground surface indicated as 'H' in Fig. 23 came to a standstill. 2) The penetration resistance increased rapidly, while the height of the

inside ground surface stood at about 475 mm. 3) From 1260 to 1300 mm in depth, the penetration resistance stopped increasing, and kept a constant value. In the meantime, H increased gradually; however, the increment of H was less than the increment of the pile penetration depth. 4) After the depth exceeded 1300 mm, the penetration resistance resumed increasing. At this stage, the increment of H was equal to the increment of the depth, that is, the inside soil and the open-ended pile itself penetrated into the model ground as one body.

Thus, the open-ended pile could not continuously remain in the full plugging condition, and intermittent plugging was observed. This sort of phenomenon has already been reported by Hight et al. (1996) who also conducted other types of model tests. In their investigation, submerged sand columns were pushed up from their base inside steel pipe piles using a rigid platen, and the load-displacement relationship for the sand plug was obtained by monitoring the load on the platen and its displacement. It is noteworthy that the identical behavior was observed in different types of model tests.

Cone penetration tests

Figures 24 and 25 display the vertical distribution of the cone penetration resistance of the ground inside the model pile obtained before and after the periodical change in pile penetration resistance appeared. In other words, Figs. 24 and 25 indicate cone resistance distributions before and after the plugging effect developed, respectively.

In the case of the unplugged pile (see Fig. 24), there were two peaks of cone resistance at 800 mm and 1250 mm in depth. The first peak at 800 mm seems to have been caused by the influence of the pile wall. The origin of the second peak is presumed to be the compression beneath the bottom tip of the model pile accompanied by the pile driving.

On the other hand, there was only one peak of the cone penetration resistance at the center of the ground inside the plugged pile, as shown in Fig. 25. The peak appeared just beneath the bottom tip of the model pile. Moreover, the maximum cone resistance of the ground inside the plugged pile was much larger than that of the ground inside the unplugged pile indicated in Fig. 24.

Thus, it was found that the vertical distribution of cone penetration resistance differed completely between the case of unplugged piles and plugged piles.

Many series of cone penetration tests have also been conducted in the ground around model piles. Figures 26 and 27 indicate the vertical distribution of cone penetration resistance at a distance of 10 cm from the wall of the model piles. Figures 26 and 27 show the cone resistance distribution obtained before and after the plugging effect took place; that is, the cyclic change of the pile penetration resistance is revealed, respectively.

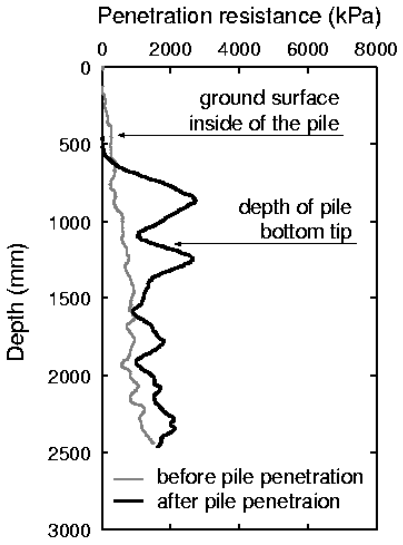

Fig. 24. Vertical distribution of cone penetration resistance of the ground inside an unplugged pile.

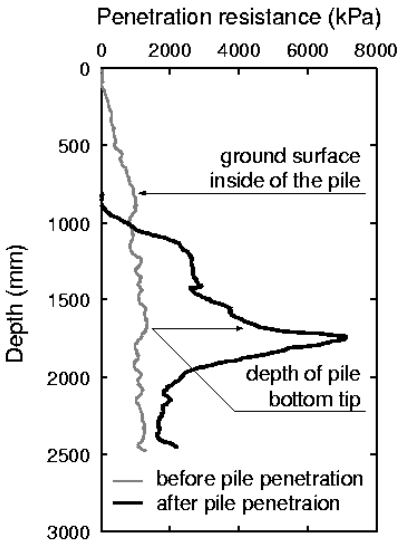

Fig. 25. Vertical distribution of cone penetration resistance of the ground inside a sufficiently plugged model pile.

Figure 26 indicates that there was no difference in the distribution of cone penetration resistance observed before and after setting up the model pile without plugging effect. On the other hand, considerable difference was found in the cone resistance before and after setting up the model pile that was sufficiently plugged, as shown in Fig. 27. According to the figure, the cone penetration resistance decreased in the shallow area of the model ground, but increased at a greater depth than the bottom tip of the model pile. The reduction of cone resistance in the shallow area was due to sand dilatancy

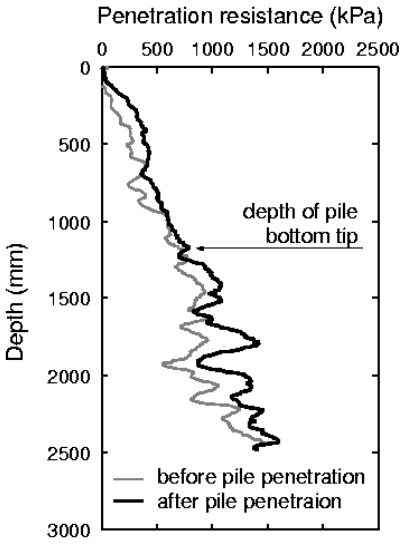

Fig. 26. Vertical distribution of cone penetration resistance at 10 cm from the wall of unplugged open-ended model pile.

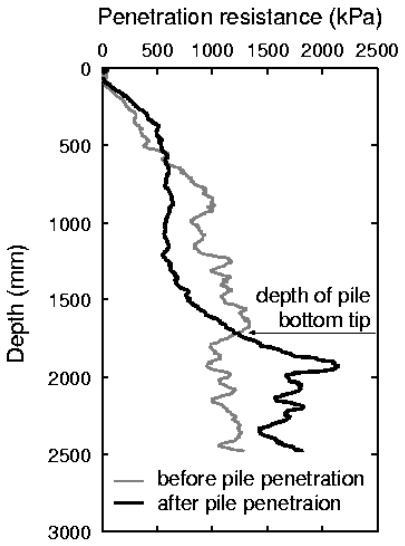

Fig. 27. Vertical distribution of cone penetration resistance at 10 cm from the wall of sufficiently plugged open-ended model pile.

caused by the large deformation following pile driving. In addition, the cone resistance increased in the deep area because the subsoil was compressed by the pile driving.

Figure 28 shows the vertical distribution of cone penetration resistance at 10 cm from the wall of the close-ended model pile. Comparing Figs. 27 and 28, it was found that the vertical distribution at 10 cm from the pile wall after setting up the model pile was very similar between the open-ended and close-ended model piles, if the open-ended pile was sufficiently

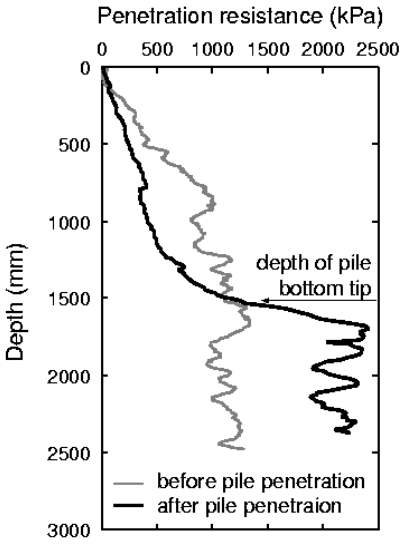

Fig. 28. Vertical distribution of cone penetration resistance at 10 cm from the wall of close-ended model pile.

plugged. However, both the reduction of cone resistance in the shallow area and the increase in the deep area were larger in the case of the close-ended pile compared to the open-ended pile. The cause was supposed to be that some installation depth was necessary for the plugging effect to develop. Before the plugging effect had developed, there was no change in the cone resistance; in other words, the ground around the pile was not affected by the pile driving (see Fig. 26). Therefore, there was no difference in cone resistance before and after pile driving in a surface layer less than 500 mm in depth, even if the open-ended pile was sufficiently plugged (see Fig. 27).

Figure 29 displays the vertical distribution of cone penetration resistance at a distance of 20 cm from the wall of an open-ended pile with the plugging effect developed. A reduction in cone resistance in the shallow area was observed; however, the increment of cone resistance in the deep area was not. Consequently, the horizontal range of the area in which the reduction of cone resistance following ground deformation was observed was larger than that of the area in which the increment of cone resistance was observed following ground compression. Needless to say, these horizontal ranges depend on the ground characteristics, especially the density of the ground. Because dense sand is more dilative, the horizontal range of the area in which the cone resistance reduction appears will be larger, and that of the area in which the cone resistance increment occurs will be smaller in the denser ground.

Change in cone penetration resistance was also checked in the field. In the loading test described in “examination of bearing capacity mechanism of open-ended piles”, CPT tests were conducted on original ground and on the ground inside the pile. CPT tests for the ground inside the pile were conducted after the pile loading tests. Figure 30 shows a comparison of CPT test data (q_c and f_s) (Nishimura et al. 2005). In this case, the

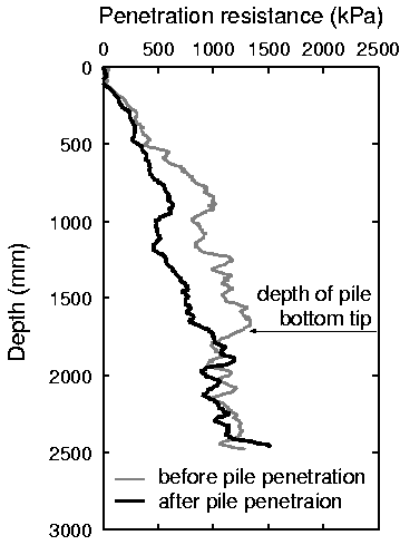

Fig. 29. Vertical distribution of cone penetration resistance at 20 cm from the wall of sufficiently plugged open-ended pile.

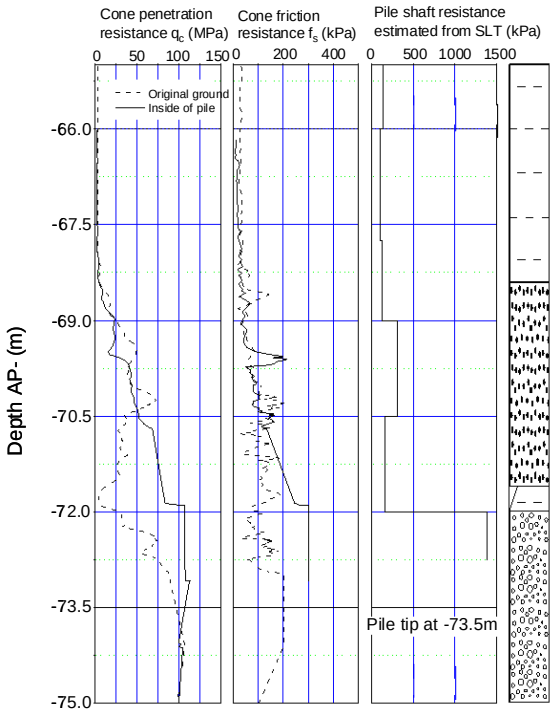

Fig. 30. CPT test results for both original ground and ground inside Pile No. 4. Right figure shows the shaft friction distribution estimated from static loading test.

outer diameter of the pile was 1500 mm. The pile tip was located at AP-73.5 m. Tip resistance of CPT (qc) was larger in the ground inside the pile compared to the original ground for a height from the pile tip to around 2D higher than the pile tip. Frictional resistance of CPT was also larger for the ground inside the pile than for the original ground in the same zone.

As shown in the right figure of Fig. 30, unit shaft resistance estimated from the static loading test increased sharply from a depth of AP-72 m. This sharp increment includes outer and inner friction. This depth coincides with the increment of CPT resistance in the ground inside the pile. This result means that there is a relationship between the increment of cone resistance and increment of shaft resistance. That is, there is a relationship between the increment of inner friction and that of cone resistance.

OBSERVATION OF DEFORMATION OF SURROUNDING GROUND DURING PENETRATION OF OPEN-ENDED PILE USING MICRO-FOCUS X-RAY CT SCANNER

Investigation so far shows the plugging occurrence situation of an open-ended pile and the change of ground when a plug is formed in an open-ended pile. A plug in the pile tip part occurs under the effect of the interaction between the pile and the ground. Therefore, it is necessary to know the deformation situation of the ground near the pile tip. As there is little available data on the situation of the ground near a pile tip during pile loading, observation of the inner ground was conducted using a micro-focus type X-ray CT scanner.

The X-ray CT scanner introduced in the Port and Airport Research Institute (PARI) in 2004 is the micro-focus type. Figure 31 shows an overview of the apparatus and Table 6 lists the basic specifications. The voltage and current can be changed manually and the distance between the X-ray tube and test piece or image intensifier can be adjusted. Therefore, the micro-focus X-ray CT scanner is very flexible and can be used for scanning a wide variety of specimens. Its very small focus achieves a high resolution that enables small parts to be easily observed, and its maximum magnification is about 80. To obtain more precise data, 6000 views can be taken in a full scan of the specimen for one cross section. Furthermore, its 3D cone-beam imaging function makes it possible to obtain consecutive images of specified cross sections. The resolution of CT images captured

Fig. 31. Overview of micro-focus X-ray CT scanner at PARI.

Table 6. Specifications of micro-focus X-ray CT in PARI.

X-ray unit	Type	Non-enclosed
	Voltage	30 – 225 kV
	Current	10 – 1000 μA
	Maximum output	135 W
	Minimum focus size	4 μm
	X-ray irradiation angle	60 deg. In cone shape
Image intensifier	Field-of-view diameter for input window	9/7.5/6/4.5 inches (selectable)
Test samples	Maximum mounting dimensions	ϕ 250 × 800 mm
	Maximum weight	600 N
X-ray shield box	Dimensions	2150 × 1310 × 2400 mm
	Weight	45100 N

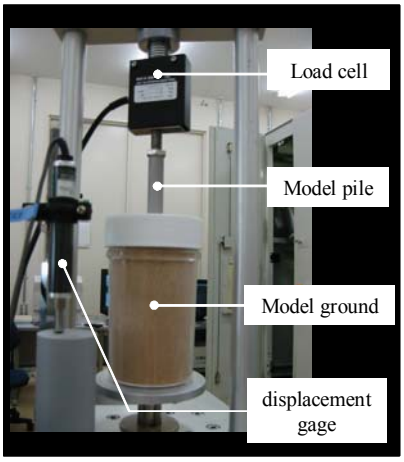

Fig. 32. Experimental setup for penetration test.

by this method is slightly lower, but the scanning time is shorter and the resolution is still acceptable for the purpose of our analysis. In each voxel (volumetric pixel), a gray level (GL) value is allocated by CT analysis. The GL value is a kind of contrasting parameter used for imaging processing, and is basically a linear parameter for estimating the density of the specimen.

The experimental setup is shown in Fig. 32. Unconfined compression apparatus was used for this vertical penetration experiment, and penetration resistance and depth were measured at the pile top. Stainless pipe pile (outer diameter: 16 mm, length: 80 mm, thickness: 0.3 mm) was used in the experiment. Dry Toyoura sand (D_{50} = 0.2 mm, U_c = 1.6) was used for the model ground. Dry sand with 5, 70, and 98% relative density was packed in an acrylic container (inner diameter: 85 mm, height: 160 mm), and ground height was adjusted to 150 mm. The pile was driven into the ground at the rate of 1 mm/min. The pile penetration experiment was conducted outside the X-ray CT scanner room. When the pile had penetrated to about 30 and 60 mm, the load was released and the container was moved into the CT room, and X-ray CT scanning was performed.

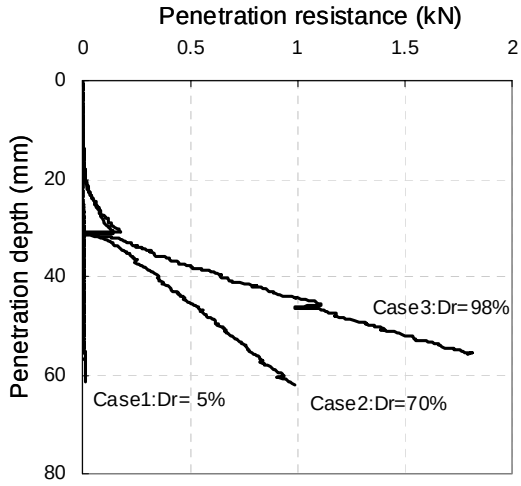

Fig. 33. Relationship between penetration resistance and depth.

The influence of penetration resistance on the state of plugging phenomena observed from CT images was considered. The relationship between penetration resistance and depth is shown in Fig. 33. The penetration resistance is proportional to the relative density of the model ground.

Figure 34 shows a vertical section of CT images selected to obtain views through the central axis of the pile at the each depth. White lines represent the pile, and gray area is sandy ground, and the black part in the pile is air. The top of the CT images shown in Fig. 34 is the ground surface. From Fig. 34, the smaller the relative density was, the larger the depression of inner ground. On the other hand, from Fig. 33, the penetration resistance of the pile was the higher when the relative density was the higher. These results mean that it was easy for a plug to develop when the relative density was low and it was difficult to make plug when the relative density was high. But there was no relationship between in plugging and bearing resistance. of piles. Bearing resistance of the pile was governed by the resistance of the ground under the pile tip. That is, the plugging phenomenon at the pipe pile tip depends on the balance between the of ground reaction and frictional resistance inside the of pile inside and the weight of the soil.

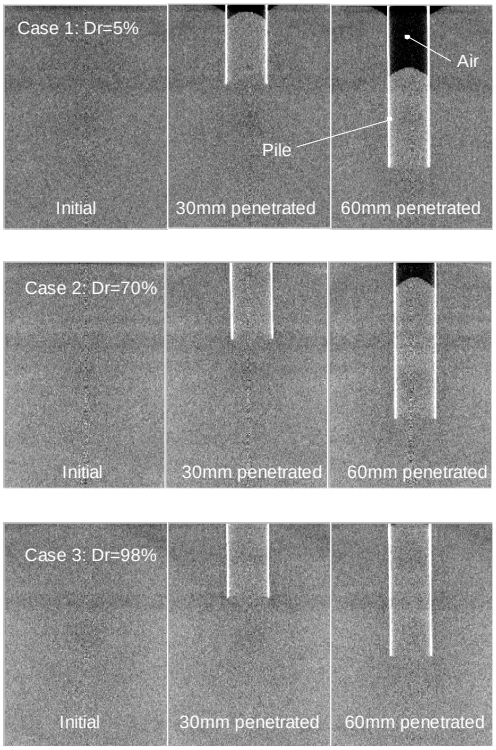

Fig. 34. Pile penetration under different relative density ground.

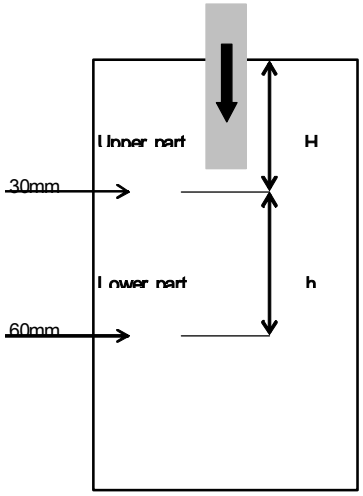

Fig. 35. Image of the experiment and target position.

To observe ground movement in the simplest way, target layers were set in the sandy layer. The target used in this series was placer iron contained in Toyoura sand and collected by magnet. Placement was 30 and 60 mm deep in the model ground. The relative density of the ground was set to 65%. The maximum depth of pile penetration was 70 mm, and X-ray CT scanning was performed at pile penetrations of 0, 30, 55, 60, and 70 mm. The other conditions were the same as before. Figure 35 shows an image of the experiment and the target.

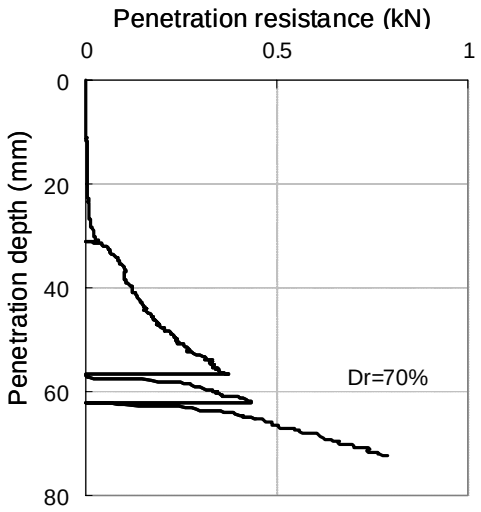

Fig. 36. Relationship between penetration resistance and depth.

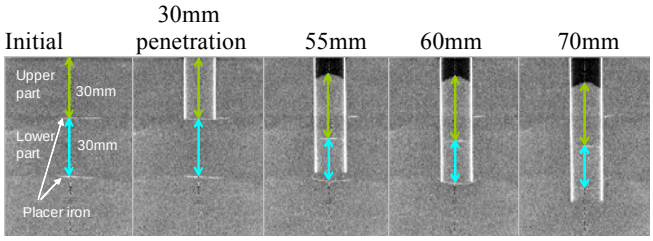

Fig. 37. Vertical image of pile penetration and movement of placer iron.

The relationship between penetration resistance and depth is shown in Fig. 36. Penetration resistance was very small up to a penetration depth of 30 mm. Later, it increased rapidly until 70 mm where penetration finished.

Figure 37 shows a vertical cross section of CT images. The two white horizontal lines are the placer iron targets as shown in Fig. 35. In these photos, the top of the images is at the ground surface. Up to a penetration depth of 30 mm, no change was observed in the target position and no settlement was observed in the inner soil. At a penetration depth of 55 mm, the inner soil settled and the thickness of the lower part of the soil inside the pile was shortened, while the thickness of the upper part never changed. Until 70 mm of penetration, the surface of the inner soil continuously settled and compression of inner soil was not observed. As seen in the right side photo, placer iron targets at 60 mm in depth penetrated into the pile. This means that settlement of the inner soil was smaller than penetration of the pile between 55 and 70 mm in depth.

From the distance change, the axial compression strain of the upper and lower parts was calculated and the relationship between penetration depth and axial strain is shown in Fig. 38. As seen in the figure, compression of the lower part occurred

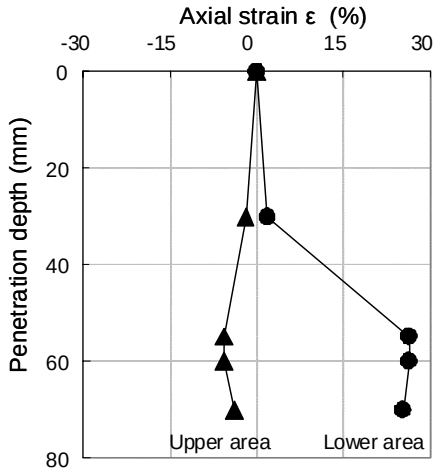

Fig. 38. Relationship between axial strain and penetration depth.

only when the pile had penetrated from 30 to 55 mm. This means that only the ground around the pile tip was compressed, although lateral ground motion could not be measured in this case.

Ground behavior around the pile tip

Referring to the above series of experiment results, a series of detailed pile penetration experiments was conducted. Exclusive penetration apparatus was prepared for improved accuracy. Aluminum piles (outer diameter: 15 mm, length: 140 mm) were used in the experiment. The thickness of the open-ended pile was 1 mm. Toyoura sand (D_{50} = 0.2 mm, U_c = 1.6) was used for the model ground. In order to investigate the movement of the ground from X-ray CT scanning results, a layer of iron particles (diameter: 0.3 mm) was used. Dry Toyoura sand of 65% relative density was packed in an acrylic container (inner diameter: 100 mm), and the ground height was adjusted to 270 mm. An overburden pressure of 2.5 kPa was applied using stainless steel balls (diameter: 2 mm). The piles were driven into the ground at a rate of 1 mm/min and maximum penetration depth was 81 mm. The entire pile penetration experiment was conducted in the micro-focus X-ray CT scanner room, as shown in Fig. 39. When the piles had penetrated to about 35 and 70 mm, pile penetration was stopped, the load was released, and extension rods were added. To obtain CT images during the experiment, pile penetration was stopped at intervals of 3 mm, and X-ray CT scanning was performed after the head load became stable.

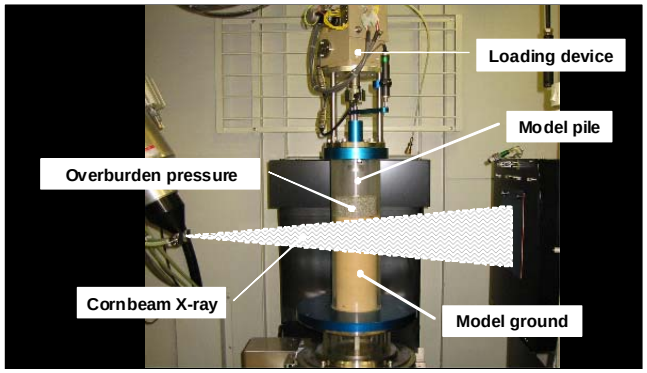

Fig. 39. Penetration test in X-ray CT room.

The relationship between penetration resistance and depth is shown in Fig. 40. One of the distinct features of the bearing capacity of the open-ended pile is that the penetration resistance did not occur at the beginning of penetration, and it decreased and increased with penetration as in the penetration depth from 55 to 65 mm. The penetration resistance of the open-ended pile started increasing from a penetration depth of 18 mm, and from that point, the increment of penetration resistance in both cases was almost equal. Around a penetration depth of about 55 mm, the resistance of the open-ended pile became almost the same as that of the closed-ended pile. This means that sufficient plugging of the open-ended pile may have developed with the

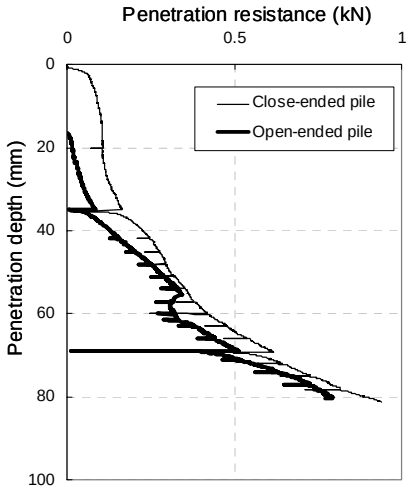

Fig. 40. Relationship between penetration resistance and depth.

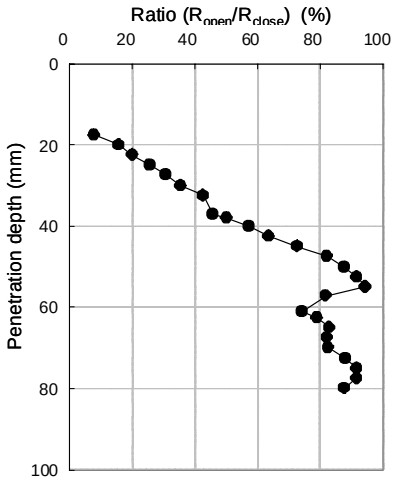

Fig. 41. Ratio of penetration resistance.

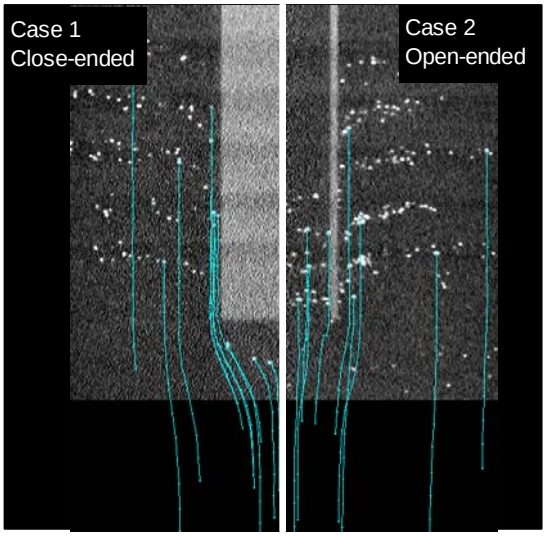

Fig. 42. Vertical section of CT image.

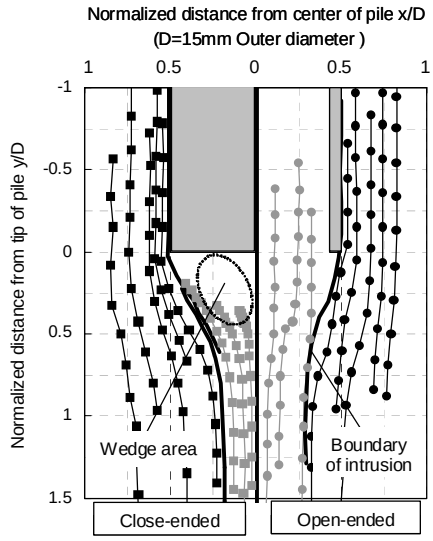

Fig. 43. Movement of particles.

depth. The resistance of the open-ended pile decreased and increased in the course of penetration at about 55 to 60 mm of penetration depth due to corresponding changes in the plugging effect. In other words, these results suggest that full plugging was not continuous; a plug formed and broke repeatedly during pile penetration. This phenomenon was also reported in "penetration experiment of open-ended piles in model ground".

Figure 41 shows the ratio of penetration resistance of the close-ended pile to that of an open-ended pile at the same depth of penetration. Because resistance did not occur in the open-ended pile at the beginning of penetration, the ratio of penetration resistance was small at first, but increased sharply after resistance occurred.

Figure 42 shows a vertical section of CT images selected to obtain views through the central axis of both pile types at the end of pile penetration at about 81 mm of penetration depth. The close-ended pile is shown on the left, and the open-ended pile, on the right. The light gray parts in the central part of the figure are the model piles. The small white points are iron particles. The lines show the routes of these particles during pile penetration from 42 to 81 mm. The image shown in this figure was taken under the condition of a fixed pile position. The particles below the pile were pushed to the outside of the pile, and this behavior decreased in proportion to the distance from the pile.

Figure 43 shows the movement of the particles with points and lines as extracted from the CT images. The points are the positions of the particles relative to the pile at each 3-mm step of penetration, and the lines are the particle routes. With the close-ended pile, the particles below the pile showed a tendency to be pushed out to the outside of the pile tip. A clear wedge existed here, and the soil was unable to intrude in this area. Some of the particles below the pile were caught at the surface of the wedge, and some were discharged to the side of the pile at the edge and then moved along the pile. Because the wedge was unified with the penetrating pile, the relative movement of soil at the surface of the wedge differed greatly. This implies that a shear zone may have developed at the wedge surface. On the other hand, in the case of the open-ended pile, the movement of particles below the pile differed in that the particles were able to move upward and penetrate into the pile. The particles outside the pile were pushed out to the outside of the pile tip.

The distribution of the change in volume tendency at the tip of the piles was estimated from the relative displacement of the particles, as shown in Fig. 44. Because the movement of particles around the piles was three dimensional, it was not possible to trace every particle from initial to final position. But in this case, the vertical sectional CT images selected were through the central axis and most particles on this plane were to be considered on the same plane. The area of some small cells, which were composed of four neighboring particles, was used to calculate the volume at each step of penetration. Each cell was assumed to possess axial symmetry, and the volume of each cell was calculated using the area and center gravity of the cell. There were wedge-shaped zones that displayed a tendency towards compaction below both the open- and close-ended piles, and there were also dilation zones at the bottom of both wedges. Dilation zones encased compaction wedges below the pile tips.

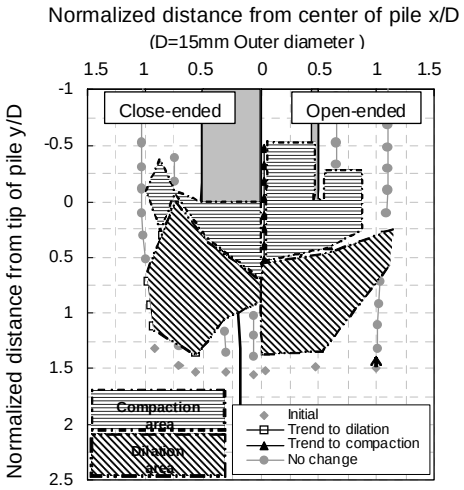

Fig. 44. Distribution of change in volume tendency.

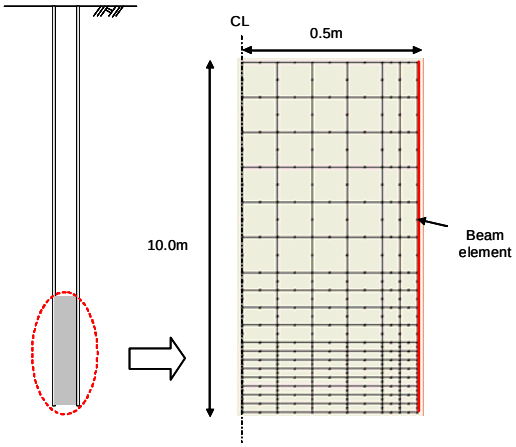

Fig. 45. Model used for analysis.

The behavior of the surrounding ground at the position of the pile tip was discussed for open-ended and close-ended piles based on a static penetration test. During the penetration experiment, movement of the surrounding ground was observed using a micro-focus X-ray CT scanner. Knowledge of the ground behavior at the pile tip and change in volume in this region was obtained by tracing iron particles that were mixed into the model ground. The following conclusions were drawn:

(1) Even if test results show similar penetration resistance, the ground behavior below an open-ended pile tip differs greatly from that below a close-ended pile tip. Although a wedge continuously exists in the area below the close-ended pile, the wedge that forms below an open-ended pile exists discontinuously. The soil below the open-ended pile enters the pile intermittently and may be compacted from the wedge area to the inside of the pile.

(2) Part of the soil below the wedge shows a tendency to be pushed out to the outside of the pile. For this reason, the soil below the wedge has a tendency to dilate.

NUMERICAL ANALYSIS ON THE STRESS INSIDE A PILE

Base bearing capacity was affected by ground conditions and pile diameter, because they affect the easiness of a plug developing. Here, the effect of dilatancy characteristics of soil on pile plugging was studied by numerical analysis.

Figure 45 shows the model used for the analysis. The pile used in this study was a steel pipe pile 1.0 m in diameter. In the analysis, the modeled zone of the pile was 1.0 m at the toe where the soil had penetrated. Polar coordinate system was used in the analysis. Half the pile was modeled and steel pipe pile was modeled as the beam element at the right end of the mesh. To consider the frictional resistance between pile and soil, joint elements were set between the pile wall and the soil.

Figure 46 shows the boundary conditions for the analysis. Displacement of the x-axis was fixed at the left end of the mesh. The x- and y-axis and rotation angle were fixed at the top of the right end point. Penetration of the soil at the pile toe was applied by displacement. Maximum upward displacement was 0.1 m.

The inner soil was modeled as super- and sub- loading model to simulate the compression and expansion characteristics of the soil, because these characteristics greatly affect the extent of occurrence of inner friction resistance. Input parameters in the analysis are shown in Table 7. Initial conditions of the analysis are shown in Table 8. Case 1 was selected as loose packed conditions and Case 2 was dense packed conditions.

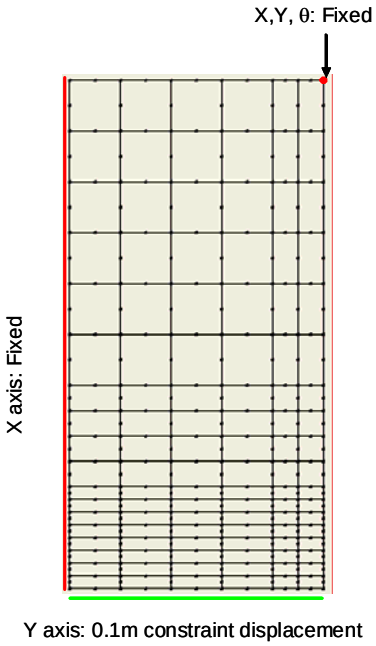

Fig. 46. Boundary conditions.

Table 7. Input parameters

Elasto-plastic parameters	
Compression index: λ	0.05
Swelling index: κ	0.012
Critical state constant: M	1.00
Intercept of NC line: N which is specific volume (f = 1 + e0) on the NC line of remolded clay at p' = 98 kPa	1.98
Poisson's ratio: ν	0.3

Evolution parameters	
Degradation parameter of structure: a (b = c = 1.0)	2.2
Degradation parameter of overconsolidation state: m	0.06
Evolution parameter of β: br	3.5
Limit of rotation: mb	0.7

Figure 47 shows the relationship between void ratio and subgrade reaction at pile toe for a displacement of 0.1 m. Subgrade reaction at a void ratio of 0.79 was 6 times larger than that of 1.08. This difference was because of the difference in dilatancy characteristics of the soil.

Table 8. Initial values of the analysis

	Case 1	Case 2
Void ratio e (Dr)	1.08 (0%)	0.79 (69%)
Initial value of structure: 1/R*	69.89	1.26
OCR: $1/R_0$	1.25	39.65
Initial slope of axis rotation: ζ_0	0.010	0.045

Figure 48 shows the horizontal stress distribution at the inner pile surface in both Case 1 and 2. In Case 1, the apparent horizontal stress increment was only seen in the zone between the pile toe and 1 m higher than the pile toe. On the other hand, in Case 2, the apparent stress increment was seen at almost all depths where soil penetrated. The other feature was the difference in the stress level. In Case 2, the maximum horizontal stress at a displacement of 0.1 m was about 5 times greater than in the same displacement in Case 1.

Figure 49 shows the vertical distribution of the increment of horizontal stress acting on the inner surface of the pile when the soil penetrated 0.1 m inside the pile. The value of α indicated on the x-axis was calculated from the ratio of horizontal stress when the soil penetrated 0.1 m inside the pile σ_x to original horizontal stress σ_{x0}. In Fig. 49, a small increment of horizontal stress was observed at only 1 m in length in Case 1 (loosely packed conditions). On the other hand, the increment of horizontal stress was large and the stress increased zone expanded to the upper part in Case 2 (densely packed conditions).

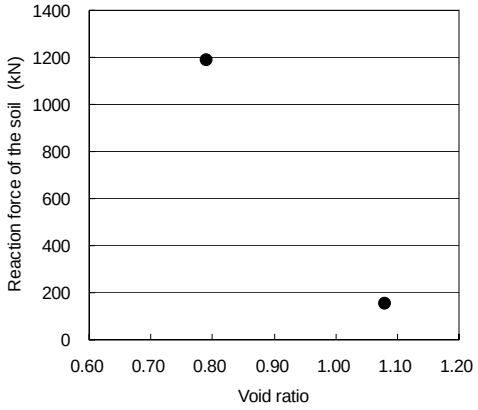

Fig. 47. Difference in subgrade reaction at pile toe in accordance with difference in void ratio.

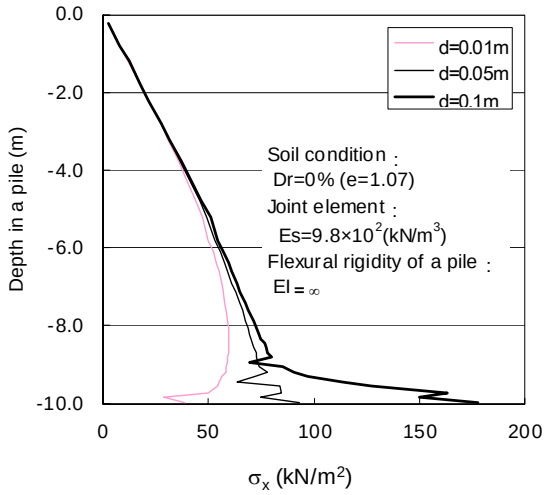

a) Case 1 (Dr = 0%)

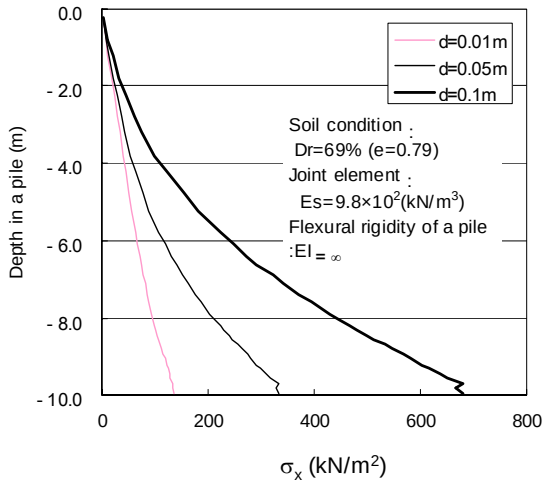

b) Case 2 (Dr = 69%)

Fig. 48. Horizontal stress distribution at inner pile surface.

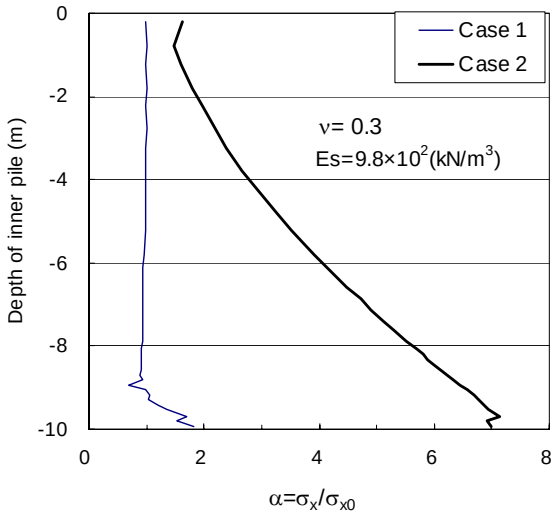

Fig. 49. Distribution of the ratio of the increment of horizontal stress σ_x/σ_{x0}.

Although earth pressure acting on the inner surface of the pile increased due to soil penetration, incremental stress value and increased zone changed greatly due to ground conditions. Therefore, it is necessary to study the change in earth pressure inside the pile in detail when applying a load for evaluating the inner friction resistance of an open-ended pile.

CONCLUSION

This study introduced the present state of pile foundations used in Japan's port facilities. Also presented was an international comparison of methods for evaluating bearing capacity used in design, which is particularly important for open-ended piles. Four different approaches were used in this study: field loading tests on real piles, laboratory experiments on model open-ended piles, small-scale pile penetration experiments for observing ground deformation, and numerical analysis of soil penetrating into a pile.

Following are the conclusions reached in this study:
(1) The resistance of a pile body reached nearly the maximum level at a small level of settlement of the pile end (about 3% of the pile diameter), while inner friction resistance required further settlement to reach the maximum level.
(2) The plugging phenomenon at the pipe pile toe depends on the balance between the ground reaction and frictional resistance inside the pile and the weight of the soil.
(3) An open-ended pile could not continuously maintain the full plugging condition, and intermittent plugging was observed.
(4) From the field loading test, it was concluded that a sharp change in the axial force might have been caused by skin friction of the inner side of the pile only one or two times the length of the pile diameter from the pile toe.
(5) The increment of earth pressure acting on the inner surface of a pile and the increased zone by pile penetration in the open-ended pile was greatly affected by the ground conditions. Therefore, it is necessary to study the change in earth pressure inside the pile in detail when applying a load for evaluating the inner friction resistance of an open-ended pile.

ACKNOWLEDGMENTS

I express my appreciation to Dr. O. Kusakabe, Dr. T. Mizutani, Mr. H. Taguchi, Mr. T. Sato, Mr. H. Yamashita, and Mr. M. Mizutani for their contribution to the research studies in this paper. Part of this study was supported by the Japan Iron and Steel Federation.

REFERENCES

Architectural Institute of Japan [2001]. "*Recommendations for the Design of Building Foundations*". p. 207 (in Japanese).

ASCE. [1993]. "*Design of Pile Foundations. Technical Engineering and Design Guides as adapted from the US Army Corps of Engineers*". No. 1, pp. 17-22.

Fleming, W.G.K., A.J. Weltman, M.F. Randolph and W.K. Elson [1992]. "*Piling Engineering 2nd edition*". Blackie, Glasgow.

Japan Road Association. 2002. *Specifications and Comments for Highway Bridges* Vol. IV Substructures (in Japanese).

Japanese Association for Steel Pipe Piles [2000]. "*Steel pipe pile – its design and construction*", p. 130 (in Japanese).

Japanese Geotechnical Society. [1999]. "*3.4 Pile foundations*". *Hand book for Geotechnical Engineering*. pp. 783-872. Japanese Geotechnical Society (in Japanese).

Japanese Geotechnical Society. [2002]. "*Standard for Method for Static Axial Compressive Load Test of Single Piles*". JGS1811-2002.

Kitajima, S., S. Kakizaki, Y. Hanaki and H. Tahara [1967]. "*On the axially bearing capacity of single piles*". *Technical note of the Port and Harbour Research Institute*, No. 36, 66 p. (in Japanese).

Meyerhof, G.G. [1956]. "*Penetration tests and bearing capacity of cohesionless soils*". *Journal of SMFE*, Vol. 82, No. SM1, pp. 1-10. ASCE.

Meyerhof, G.G. [1957]. "*Discussion on soil properties and their measurement*". *Discussion 2. Proc. of the IV International Conference on SMFE*, Vol. III, p. 110. ASCE.

Meyerhof, G.G. [1959]. "*Compaction of sands and bearing capacity of piles*". *Journal of SMFE*, Vol. 85, No. SM6, pp. 1-29. ACSE.

Nicola, A. and Randolph, M.F. 1997. "*Plugging behaviour of driven and jacked piles in sand*". *Geotechnique* 47(4): 841-856.

Nishimura, N., O. Kusakabe, Y. Kikuchi, J. Fukui, H. Sasaki, and H. Geshi. [2005]. "*Cone penetration tests for inside soil of driven open-ended steel pipe piles in Tokyo port seaside road project*", *Proc. of 40th JNCGE* (in Japanese).

Overseas Coastal Area Development Institute of Japan. [2002]. "*Technical standards and commentaries for port and harbour facilities in Japan*". pp. 286-287. Daikousha.

Orr, T.L.L, E.R. Farrell. [1999]. "*Geotechnical Design to Eurocode 7*". pp. 106-113. Springer.

Yamagata, K. and K. Nagai. [1973]. "*Consideration of an open ended steel pipe pile (No. 2)*". *Journal of Architecture and Building Engineering*. No. 213 (in Japanese).

Yamagata, K. [1975]. "*Allowable bearing capacities of a pile constructed in various installation methods*". Tsuchi to Kiso. Vol. 23, No. 7, pp. 13-20. Japanese Geotechnical Society (in Japanese).

Yasufuku, N., H. Ochiai and S. Ohno [2001]. "*Pile End-bearing Capacity of Sand Related to Soil Compressibility*". *Soils and Foundations*, Vol. 41, No. 4, pp. 59-71. Japanese Geotechnical Society.

Vesic, A.S. [1972]. "*Expansion of Cavities in Infinite Soil Mass*". *Journal of SMFE,* Vol. 98, No. SM3, pp. 265-290, ASCE.